Spatial filtering in ambient noise interferometry

Olivier Carrière,[a] Peter Gerstoft, and William S. Hodgkiss
Scripps Institution of Oceanography, University of California San Diego, La Jolla, California 92093-0238

(Received 21 June 2013; revised 9 January 2014; accepted 16 January 2014)

Theoretically, the empirical Green's function between a pair of receivers can be extracted from the cross correlation of the received diffuse noise. The diffuse noise condition rarely is met in the ocean and directional sources may bias the Green's function. Here matrix-based spatial filters are used for removing unwanted contributions in the cross correlations. Two methods are used for solving the matrix filter design problem. First a matrix least-square problem is solved with a low-rank approximation of the pseudo-inverse, here, derived for linear and planar arrays. Second, a convex optimization approach is used to solve the design problem reformulated with *ad hoc* constraints. The spatial filter is applied to real-data cross correlations of elements from a linear array to attenuate the contribution of a discrete interferer. In the case of a planar array and simulated data, a spatial filter enables a passive upgoing/downgoing wavefield separation along with an efficient rejection of horizontally propagating noise. The impact of array size and frequency band on the filtered cross correlations is discussed.
 [http://dx.doi.org/10.1121/1.4863658]

PACS number(s): 43.60.Gk, 43.30.Pc, 43.60.Fg, 43.30.Nb [ZHM] Pages: 1186–1196

I. INTRODUCTION

In ocean acoustics, surface-generated noise constitutes a natural source of illumination propagating in all directions[1] and covering a large frequency band (10 Hz–50 kHz). It is well established that the cross correlation of a diffuse noise field observed by a receiver pair provides an estimate of the Green's function between this pair, also called the empirical Green's function (EGF), as shown theoretically and experimentally.[2–4] The surface-generated noise can be recorded using passive arrays of sensors and processed to estimate the EGF between pairs of receivers.[5] In this paper, we derive data-independent spatial filters for improving estimates of the EGF for one-dimensional (1D) and two-dimensional (2D) horizontal arrays.

In practice, EGF extraction from ambient noise is affected by several artifacts: (i) Surface generated noise usually is modeled as an infinite 2D plane sheet of sources. Contrary to a volume noise model, this gives a one-sided illumination as the noise sources do not surround the receivers, which leads to spurious events[5] or asymmetry[6] in the EGF. (ii) Surface noise anisotropy[7,8] and a limited frequency band[9] also affect the cross correlations, and thus the EGF. (iii) Noise in the lower part of the spectrum (up to 300 Hz) usually is dominated by ship noise. If loud localized sources are present in the environment, the cross correlations might be dominated by the arrivals coming from these sources and lead to biases in the travel time estimates.[10–12]

Array processing methods have been proposed for correcting bias in source distribution for cross correlation purposes.[13,14] In Ref. 13, horizontally propagating noise inhomogeneity was compensated by a *passive inverse filter*. In Ref. 14, spatio-temporal filters are constructed using the first singular vectors of a reference cross-spectral density matrix (CSDM). Their filters were shown to improve the emergence rate of cross correlation peaks between two vertical arrays, and are data (or model) dependent.

Here, we consider the use of a single horizontal array of receivers (1D or 2D) and apply spatial filtering to attenuate unwanted propagating noise contributions in its CSDM. The spatial filter design is directly related to discrete Fourier transform and frequency (or wavenumber) sampling. These topics are discussed extensively in the digital signal processing literature (see, e.g., Ref. 15). The classical formulation of the filter design leads to a least-square problem. As the wavelength sampling varies with frequency (for a given receiver spacing along the array), the least-square inversion has to be restricted to the degrees of freedom of the array to remain stable below the design frequency. For this purpose, a singular value decomposition (SVD) of the frequency-dependent steering matrix is used, following Refs. 16–18. Analytic expressions of the SVD spectrum and stable truncation points are derived mathematically here for 1D and 2D arrays.

Alternatively, a matrix filter also can be formulated as the solution to a convex optimization problem.[19] In the convex optimization approach, the stability is controlled by the constraints used in the definition of the optimization problem so that no SVD truncation is required. Convex optimization gives more flexibility to the filter designer by providing more control parameters than a standard least-square inversion. However, the finding of a stable solution depends on the control parameter values and might require some tuning steps. Convex optimization already has been applied for data-independent beampattern optimization[20] and for finite impulse response filter.[21] Here, we restrict the use of convex optimization to 1D array spatial filters to maintain reasonable computational times and discuss differences from the least-square approach.

A 2D array has the important property of being able to point in a single direction (azimuth and elevation) without suffering from cylindrical ambiguity around the (1D) array axis (the so-called *cone* angle). Contrary to vertical arrays,

[a]Author to whom correspondence should be addressed. Electronic mail: olivcarriere@gmail.com

beamforming with horizontal arrays of hydrophones cannot separate up- and downgoing waves. However, combining collocated hydrophones and vertical particle velocity sensors, e.g., with an ocean bottom sensor (OBS) network, enable an up/down separation scheme[22,23] which, combined with beamforming, provide an acoustic or seismic data measurement system able to point in *any* direction (not necessarily vertical) or filter unwanted direction of arrival, with a resolution related to the beampattern. By implementing a spatial filter that attenuates horizontally propagating noise, the subsurface reflection peaks in the EGF are enhanced. The combination of beamforming and cross correlation using vertical arrays is discussed in Refs. 24 and 25.

2D planar arrays are common in the seismic community, in land (e.g., USArray stations[26]) as well as underwater (e.g., the permanent ocean-bottom array at the Valhall Field[27]), but they are not yet common in ocean acoustics. Keeping in mind the scale difference (frequency, medium propagation speed, and receiver spacing), the present results might be of interest for spatial filtering of identified events or rejection of specific propagating waves for seismic applications.

The remaining parts of the paper are organized as follows. Section II starts with the basic principles of EGF extraction from the CSDM and spatial filtering. Section III describes a convex optimization approach to solve the spatial filter design problem. Then, in Sec. IV, the expression for a stable matrix-based filter with a 1D array is derived in the SVD context, leading to an identical truncation condition as obtained in Ref. 17. These results then are extended for 2D planar arrays. Section V illustrates the effect of spatial filters on EGF extraction. First, experimental data with a 1D array demonstrates the attenuation of a discrete interfering source in active cross correlations. Second, an application of upgoing/downgoing noise separation is proposed with simulated data on a 2D planar array for the purpose of enhancing the subsurface reflections and attenuating the spurious arrivals. Requirements and limitations that come with spatial filters and the two presented design approaches then are discussed in Sec. VI.

II. BACKGROUND

A. Green's function extraction

The cross correlation $C_{ab}(\tau)$ of signals received on two receivers a and b, respectively located at r_a and r_b, is related to the time-domain Green's function $G(\tau, r_a, r_b)$ between these receivers,[2–4]

$$\frac{dC_{ab}(\tau)}{d\tau} \propto -G(\tau, r_a, r_b) + G(-\tau, r_a, r_b), \tag{1}$$

given that the signals received are due to a random diffuse white noise field.

In the frequency domain, the cross spectral density is given by

$$R_{ab}(\omega) = \mathcal{F}[C_{ab}(\tau)], \tag{2}$$

where $\mathcal{F}$ denotes the Fourier transform. Considering a single array of receivers, the CSDM is the mathematical expectation of the outer product of the vector $\boldsymbol{p}(\omega)$ of complex pressure on the receivers

$$\boldsymbol{R}(\omega) = \mathbb{E}\left[\boldsymbol{p}(\omega)\boldsymbol{p}(\omega)^H\right], \tag{3}$$

where the superscript H denotes the conjugate transpose. In practice, the CSDM is approximated by the sample covariance matrix (SCM), defined as the average of J outer-products of the short-time Fourier transforms of the signals

$$\hat{\boldsymbol{R}}(\omega) = \frac{1}{J}\sum_{j=1}^{J}\boldsymbol{p}_j(\omega)\boldsymbol{p}_j(\omega)^H = \frac{1}{J}\sum_{j=1}^{J}\hat{\boldsymbol{R}}_j(\omega), \tag{4}$$

where $\hat{\boldsymbol{R}}_j(\omega)$ is referred to as the short-term covariance matrix (STCM) in the following.

B. Spatial filter

Array processing can be used to spatially filter incoming signals based on their wavenumber or their impinging angle. Instead of manipulating the beamformer outputs of sub-arrays, we use matrix-based filters.[16–18] The output of a matrix-based filter has the same dimension as the input, as we are interested in extracting (or attenuating) a useful (or unwanted) part of the signal. These filters are data independent allowing pre-computation of the filter for a given sensor geometry and frequency band.

Considering signals received on an array of N receivers, $\boldsymbol{p}(\omega)$, we want to design a spatial filter $\boldsymbol{S}(\omega)$ of size $N \times N$ for removing or isolating contributions from a given direction

$$\tilde{\boldsymbol{p}}(\omega) = \boldsymbol{S}(\omega)\boldsymbol{p}(\omega), \tag{5}$$

where the filtered complex pressure, $\tilde{\boldsymbol{p}}(\omega)$, is a weighted sum of the original complex pressure over the array. Contrary to a beamformer, the output is not merged into a centered signal, removing the need of considering sub-arrays for the cross correlations. Depending on the application, a spatial notch filter or spatial bandpass filter can be designed.

We are interested in applying the spatial filters to cross correlated signals. Spatially filtered STCM are given by the outer product of spatially filtered short-term signals

$$\tilde{\boldsymbol{R}}_j(\omega) = \tilde{\boldsymbol{p}}_j(\omega)\tilde{\boldsymbol{p}}_j^H(\omega) = \boldsymbol{S}(\omega)\hat{\boldsymbol{R}}_j(\omega)\boldsymbol{S}^H(\omega). \tag{6}$$

Equivalently, the spatially filtered SCM is obtained as

$$\tilde{\boldsymbol{R}}(\omega) = \frac{1}{J}\sum_{j=1}^{K}\tilde{\boldsymbol{p}}_j(\omega)\tilde{\boldsymbol{p}}_j^H(\omega) = \boldsymbol{S}(\omega)\hat{\boldsymbol{R}}(\omega)\boldsymbol{S}^H(\omega). \tag{7}$$

Matrix-based spatial filters are obtained as follows: A frequency-dependent plane-wave steering matrix, $\boldsymbol{V}$, is composed of K replica vectors of length N. These vectors are defined as the phase advance along the N array elements, as a function of slowness (or the impinging angle, if the propagation speed is known). The spatial filter, $\boldsymbol{S}$, is designed from a constraint, $\boldsymbol{D}$,

$$\boldsymbol{SV} = \boldsymbol{VD}, \tag{8}$$

where $\boldsymbol{D} = \mathrm{diag}(\boldsymbol{d})$ is a diagonal matrix containing the idealized design coefficients in the beam space, with $\boldsymbol{d} = [d_1, \ldots, d_K]$ defined as

$$d_k = \begin{cases} 0, & \text{if } \theta_k \in \Theta_\mathrm{R} \\ 1, & \text{otherwise.} \end{cases} \tag{9}$$

A value of 1 indicates that we want to pass with a 0-dB gain arrivals from directions that are not in the rejection band, Θ_R. The design problem, Eq. (8), is solved using a convex optimization approach (Sec. III) and a least-square solution (Sec. IV).

III. CONVEX OPTIMIZATION BASED FILTER DESIGN

Vaccaro and Harrison[19] showed that the design of a matrix filter can be formulated as a convex optimization problem. Convex optimization is an attractive approach as it has a straightforward formulation, and many efficient solvers exist,[28] even for moderately sized problems (less than 1000 variables).

Instead of solving directly the design problem Eq. (8), the problem is reformulated as an optimization problem constrained with criteria for the matrix filter in the rejection (R), transition (T), and pass (P) bands (Fig. 1).

The spatial filter is the solution of the following optimization problem

$$\hat{\boldsymbol{S}} = \arg_{\boldsymbol{S}}\min \sum_r ||\boldsymbol{S}\boldsymbol{v}(\theta_\mathrm{r})||_2^2, \quad \theta_\mathrm{r} \in \Theta_\mathrm{R}$$
$$\text{subject to } \begin{cases} \max_p ||\boldsymbol{S}\boldsymbol{v}(\theta_\mathrm{p}) - \boldsymbol{v}(\theta_\mathrm{p})||_2 < \epsilon, & \theta_\mathrm{p} \in \Theta_\mathrm{P} \\ \max_t ||\boldsymbol{S}\boldsymbol{v}(\theta_\mathrm{t})||_2 \le c_\mathrm{T}, & \theta_\mathrm{t} \in \Theta_\mathrm{T}, \end{cases} \tag{10}$$

i.e., a filter that minimizes the contribution of waves impinging on the array with an incident angle in the rejected band, Θ_R, while keeping good fidelity in the passband, Θ_P ($\epsilon \approx 0$) and limiting the amplitude in the transition band ($c_T \approx 1$). Equation (10) can be replaced by a minimax criterion

$$\hat{\boldsymbol{S}} = \arg_{\boldsymbol{S}}\min \max_r ||\boldsymbol{S}\boldsymbol{v}(\theta_\mathrm{r})||_2^2, \quad \theta_\mathrm{r} \in \Theta_\mathrm{R}. \tag{11}$$

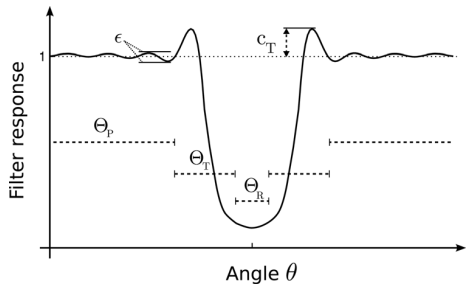

FIG. 1. Schema of a notch filter response [Eq. (32)] based on a convex optimization designed with rejection (R), transition (T), and pass (P) bands. The values of ϵ and c_T control the filter response outside of the rejection band.

The response of the filter is controlled by the passband fidelity constraint, ϵ, the transition constraint, c_T, and the width of the transition band, Θ_T. By adjusting ϵ and c_T, the notch depth can be modified without changing the transition width. Compared to a more conventional approach based on a least-square solution of Eq. (8), the convex optimization approach is more flexible thanks to the additional control parameters that are the constraint numbers.

IV. TRUNCATED LEAST-SQUARE FILTER

Despite the flexibility and the simplicity of implementation of the convex optimization approach, its computational burden is a major obstacle for very large arrays (hundreds of sensors). A straightforward method to solve the design problem Eq. (8) is given by the overdetermined least-square problem,[29] considering a number of directions larger than the number of sensors $K > N$, as

$$\boldsymbol{S} = \boldsymbol{V}\boldsymbol{D}\boldsymbol{V}^+, \tag{12}$$

where $\boldsymbol{V}^+$ (size $K \times N$) is the pseudo-inverse of the steering matrix, $\boldsymbol{V}$, defined as

$$\boldsymbol{V}^+ = \boldsymbol{V}^H(\boldsymbol{V}\boldsymbol{V}^H)^{-1}. \tag{13}$$

The pseudo-inverse is computed from the SVD of the steering matrix, $\boldsymbol{V}$. Small singular values make the pseudo-inverse unstable and thus strongly impact $\boldsymbol{S}$. Therefore, a low rank approximation of $\boldsymbol{V}^+$ is obtained by truncating singular values in the decomposition to remove the contributions of near-zero singular values. The steering matrix is of lower rank when the receiver spacing samples the spatial domain with an interval shorter than a half wavelength. Note that the opposite situation (receiver spacing larger than a half wavelength) does not require a truncation, but is affected by spatial aliasing.

Linear array (1D) or planar array (2D) designs result in different frequency-dependent truncation conditions. Using matrix-based filters on receiver arrays, a user-defined threshold[16] and the degrees of freedom of the array[17,18] previously were proposed as truncation conditions for 1D arrays. Here, a similar expression is obtained for a 1D array through derivation of the singular value spectrum and its associated truncation point. The results are further extended for 2D arrays. These two cases are treated separately in the next two sections. In the following, we use the impinging angle as the variable of interest, assuming a known propagation speed.

A. Linear array

For a 1D array, a frequency-dependent steering matrix, $\boldsymbol{V}$, discretizes the angular domain $\theta = [-\pi/2, \pi/2]$ in K directions, with $\theta = 0$ corresponding to the broadside direction [Fig. 2(a)],

$$\boldsymbol{V} = [\boldsymbol{v}(\theta_1) \cdots \boldsymbol{v}(\theta_K)]. \tag{14}$$

Each column of $\boldsymbol{V}$ is a replica vector, $\boldsymbol{v}$, defined as

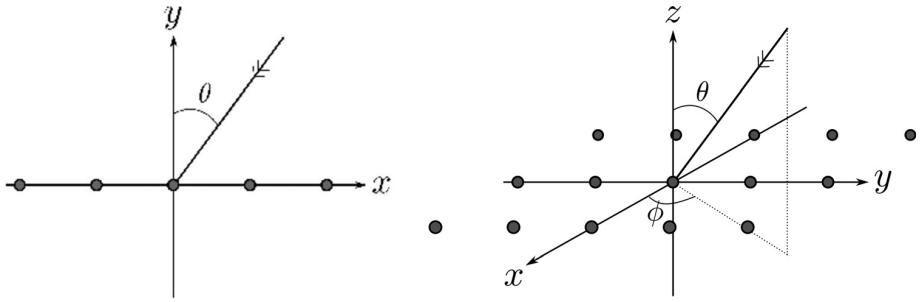

FIG. 2. (a) Linear (1D) array. (b) Planar (2D) array.

$$\boldsymbol{v}(\theta) = \begin{bmatrix} \exp\left(i\frac{2\pi}{\lambda}(x_1 \sin\theta)\right) \\ \vdots \\ \exp\left(i\frac{2\pi}{\lambda}(x_N \sin\theta)\right) \end{bmatrix}, \tag{15}$$

where λ is the wavelength. Each replica vector, $\boldsymbol{v}$, corresponds to a plane-wave impinging on the array with an incidence angle, θ.

The first N singular values ($K > N$) of the steering matrix, V, correspond to the positive square root of the eigenvalues of $Q = VV^H$. The elements of Q are given by

$$Q_{ij} = \sum_k V_{ik} V_{jk}^* = \sum_k v_i(\theta_k) v_j^*(\theta_k). \tag{16}$$

For a continuous sampling in θ, Eq. (16) is approximated by

$$\begin{aligned} Q_{ij} &\approx \frac{1}{\pi}\int_{-\pi/2}^{\pi/2} \exp\left(i\frac{2\pi}{\lambda}(\Delta x_{ij}\sin\theta)\right) \mathrm{d}\theta \\ &= J_0(2\pi\beta|i-j|), \end{aligned} \tag{17}$$

with $\Delta x_{ij} = |x_j - x_i|$, and where J_0 is the zeroth order Bessel function.

The parameter β is a dimensionless frequency, defined as the ratio between receiver spacing, δx, and wavelength, λ,

$$\beta = \frac{\delta x}{\lambda} = \frac{\omega \delta x}{2\pi c}. \tag{18}$$

A value of $\beta = 0.5$ corresponds to the design frequency (a spacing of $\lambda/2$). For $\beta > 0.5$, beamforming introduces spatial aliasing.

Equation (17) corresponds to the cross-spectrum for a 2D isotropic and uncorrelated noise field.[30,31] The matrix Q is a symmetric Toeplitz matrix. Asymptotically, the eigenvalues of a Toeplitz matrix are distributed as the samples of the Fourier transform of the *generating* function of this Toeplitz matrix,[32] given by

$$\phi(k_x) = \mathcal{F}\{J_0(2\pi\beta x)\} = \frac{1}{\pi\beta}\frac{\mathrm{rect}(k_x/4\pi\beta)}{\sqrt{1-(k_x/2\pi\beta)^2}}, \tag{19}$$

where the spatial frequency $k_x \in [-\pi, \pi[$ and $\mathrm{rect}(x)$ is 0 outside the interval $[-1/2, 1/2]$ and unity inside. For $\beta \leq 0.5$, this expression is non-zero when $|k_x| < 2\pi\beta$. As the N eigenvalues sample regularly the spatial frequency domain, $k_x \in [-\pi, \pi[$, non-zero eigenvalues have an index, n, such that[31]

$$\left|n - \frac{N+1}{2}\right| < \beta. \tag{20}$$

For sorted eigenvalues, this condition leads to a truncation index

$$n_\lambda = 2N\beta \approx \frac{L}{\lambda/2}. \tag{21}$$

This truncation reduces the number of eigenvalues to the number of degrees of freedom at each frequency, i.e., the number of half wavelengths along the array aperture, L.[17]

The spectrum of singular values for a linear array with $N = 100$ elements is shown in Fig. 3(a) for several values of β. The asymptotic curve [square root of Eq. (19)] for $\beta = 0.4$ is superimposed. For $\beta < 0.5$, i.e., at frequencies below the design frequency, the steering matrix has singular values of low amplitude (zero-valued in the asymptotic expression). For $\beta > 0.5$ (aliasing regime), the truncation index exceeds the number of singular values and therefore the spectrum does not need to be truncated.

B. Planar array

The extension to the 2D case is relatively straightforward and requires minor changes from the 1D array case. With a 2D array, the frequency-dependent steering matrix, $\boldsymbol{V}$, now discretizes the angular domain $\{\theta = [0, \pi/2] \cup \phi = [0, 2\pi]\}$ in $K \times L$ directions [Fig. 2(b)]

$$\boldsymbol{V} = [\boldsymbol{v}(\theta_1, \phi_1) \cdots \boldsymbol{v}(\theta_K, \phi_L)] \tag{22}$$

constructed with 2D replica vectors $\boldsymbol{v}$ defined as

$$\boldsymbol{v}(\theta, \phi) = \begin{bmatrix} \exp\left[i\frac{2\pi}{\lambda}(x_1 \sin\theta\cos\phi + y_1 \sin\theta\sin\phi)\right] \\ \vdots \\ \exp\left[i\frac{2\pi}{\lambda}(x_N \sin\theta\cos\phi + y_M \sin\theta\sin\phi)\right] \end{bmatrix}. \tag{23}$$

For an array of $N \times M$ sensors, each vector $\boldsymbol{v}$ is of dimension $NM \times 1$. The spatial filter design [Eq. (8)] holds

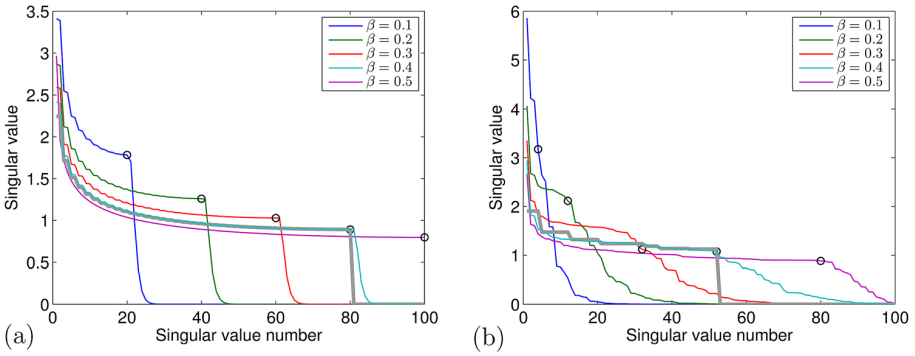

FIG. 3. (Color online) Singular value spectrum of the steering matrix for varying values of β (a) for a 1D array with 100 elements, (b) for a 2D array with 10 by 10 elements. The truncation index (circles) is given by Eq. (20), 1D case, and Eq. (30), 2D case, respectively. The corresponding sampling of the asymptotic expression [Eq. (19) for 1D case, Eq. (29) for 2D case] is shown for $\beta = 0.4$ (thick line).

for the 2D case, with a diagonal matrix D containing the coefficients $\boldsymbol{d} = [d_1, \ldots, d_{KL}]$ redefined as

$$d_{kl} = \begin{cases} 0, & \text{if } \theta_k \in \Theta_R \text{ and } \phi_l \in \Phi_R \\ 1, & \text{otherwise,} \end{cases} \tag{24}$$

where $\{\Theta_R \cup \Phi_R\}$ defines the rejection band, and the solution of the design equation is given by a set of NM least-square optimization problems.

The spectrum of the 2D steering matrix [Fig. 3(b)] differs from the 1D case. The low-rank approximation of $\boldsymbol{V}^+$ requires therefore a different truncation index. Again, we consider the eigenvalues of the matrix, $Q = VV^H$. For a continuous sampling in θ and ϕ, the elements of the matrix Q are

$$Q_{ij} \approx \frac{1}{\pi/2}\frac{1}{2\pi}\int_0^{\pi/2}\int_0^{2\pi} \exp\left[i\frac{2\pi}{\lambda}\left(\Delta x_{ij}\sin\theta\cos\phi + \Delta y_{ij}\sin\theta\sin\phi\right)\right] \mathrm{d}\phi\,\mathrm{d}\theta, \tag{25}$$

where $\Delta x_{ij} = |x_j - x_i|$ and $\Delta y_{ij} = |y_j - y_i|$. Assuming identical spacing δr in x and y directions, we can use $\beta = \delta r/\lambda$. Introducing polar coordinates,

$$\rho_{ij} = \frac{\sqrt{\Delta x_{ij}^2 + \Delta y_{ij}^2}}{\delta r}, \quad \Phi_{ij} = \arctan\left(\frac{\Delta y_{ij}}{\Delta x_{ij}}\right), \tag{26}$$

$$(\Delta x_{ij},\, \Delta y_{ij})^T = \delta r\rho_{ij}(\cos\Phi_{ij},\, \sin\Phi_{ij})^T. \tag{27}$$

We rewrite Eq. (25) using the parameter β,

$$\begin{aligned} Q_{ij} &\approx \frac{1}{\pi^2}\int_0^{\pi/2}\int_0^{2\pi} \exp[i2\pi\beta\rho_{ij}\sin\theta \\ &\quad\times\left(\cos\Phi_{ij}\cos\phi + \sin\Phi_{ij}\sin\phi\right)]\,\mathrm{d}\phi\,\mathrm{d}\theta \\ &= \frac{1}{\pi^2}\int_0^{\pi/2}\int_0^{2\pi} \exp[i2\pi\beta\rho_{ij}\sin\theta\cos(\Phi_{ij}-\phi)]\,\mathrm{d}\phi\,\mathrm{d}\theta \\ &= \frac{1}{\pi/2}\int_0^{\pi/2} J_0\left(2\pi\beta\rho_{ij}\sin\theta\right)\mathrm{d}\theta \\ &= J_0^2\left(\pi\beta\rho_{ij}\right), \end{aligned} \tag{28}$$

where the last line is obtained from a property of Bessel integrals.[33]

Because of the folding of the two components, x and y, the matrix Q has a structure of a Toeplitz block Toeplitz, i.e., a Toeplitz matrix of blocks which are Toeplitz themselves. The theorem linking the eigenvalues of such a matrix and the Fourier transform of its generating function holds,[34] and we thus have to evaluate the 2D Fourier transform of the right-hand side of Eq. (28).

The 2D Fourier transform of a radially symmetric function corresponds to its Hankel (or Bessel–Fourier) transform.[35] Its solution is deduced from Hankel transform properties,[36]

$$\begin{aligned} \phi(\kappa) &= \mathcal{F}_{2D}\left\{J_0^2(\pi\beta\rho)\right\} \\ &= 2\pi\int_0^\infty J_0^2(\pi\beta\rho)J_0(\kappa\rho)\rho\mathrm{d}\rho \\ &= 2\pi H_0\{J_0^2(\pi\beta\rho)\} \\ &= \frac{2}{\pi\beta}\frac{\mathrm{rect}(\kappa/4\pi\beta)}{\kappa\sqrt{1-(\kappa/2\pi\beta)^2}}, \end{aligned} \tag{29}$$

where $\kappa = \sqrt{k_x^2 + k_y^2}$ and k_x and k_y are in the interval $[-\pi, \pi[\times[-\pi, \pi[$. For $\beta^2 \le 0.5$, Eq. (29) is non-zero when $|\kappa| < 2\pi\beta$. For a finite number of $N_x \times N_y$ receivers, an approximate distribution of the eigenvalue spectrum thus is obtained by sampling Eq. (29).[34] Similarly to the 1D case, it follows that the 2D indexes n, m of non-zero eigenvalues satisfy the condition

$$\sqrt{\left(n - \frac{N_x+1}{2}\right)^2 + \left(m - \frac{N_y+1}{2}\right)^2} < \beta, \tag{30}$$

with $n = 1, \ldots, N_x$ and $m = 1, \ldots, N_y$, and the analogy with Eq. (20) (1D case) is obvious. Equation (30) describes the interior of an ellipse with semi-axes βN_x and βN_y. The truncation index of sorted eigenvalues is thus

$$n_\lambda = \pi\beta^2 N_x N_y \approx \frac{\pi}{4}\frac{A}{(\lambda/2)^2}, \tag{31}$$

i.e., proportional to the ratio between the area, A, covered by the array and the square of half wavelength. Note that the definition of β used implies that this truncation can be used

up to $\beta = 1/\sqrt{2}$ (instead of $\beta = 1/2$ for the 1D case). The asymptotic expression for the eigenvalue spectrum [2D case, Eq. (29)] with $\beta = 0.4$ is shown in Fig. 3(b).

V. APPLICATION EXAMPLES

Two applications illustrate the use of spatial filtering in interferometric processing. First, a notch spatial filter is used with a 1D array to mitigate the contribution of an interferer in cross correlations of active shot data. The second application with simulated data demonstrates that a spatial filter focusing a 2D array toward the vertical enables an upgoing/downgoing wavefield separation scheme for ambient noise, thereby improving subsurface imaging.

A. Interference removal from active cross correlations with 1D array

In April 2011, 15 OBS provided by Woods Hole Oceanographic Institution were deployed at the Woolsey Mound (Northern Gulf of Mexico) at 900-m water depth. Subsurface imaging based on active interferometric processing of this data set was presented in Ref. 12. A subset of these OBS formed a short line array with 11 OBS spaced ~26-m apart [Fig. 4(a)]. A gas-injection gun was towed near the surface above the OBS line, from south to north, shooting approximately every 25 m covering a 5500 m range. The sampling rate of the OBS is 200 Hz, limiting the useful frequency band to a maximum of 100 Hz. The active OBS survey was performed on April 7, from 10:01–11:03 UTC, resulting in a new shot triggered manually every 10–15 s. One-minute moving averages of broadband beamforming (implemented in the frequency domain using 2-s segments) identifies the active survey as the strong feature that goes from +70° to −70° [Fig. 4(b)]. A second feature revealed by the beamformer output is a distant seismic survey present during the whole deployment that impinges on the array with a constant angle of +40° and significant power over the whole frequency band of interest.

1. Truncated least-square filter

To mitigate the contamination of this interferer in the cross correlations, a spatial filter, $\boldsymbol{S}^{1D}$, is designed to null out arrivals impinging on the array at 35°–45°. This spatial filter is obtained using Eq. (12), where the pseudo-inverse uses the 1D truncation condition [Eq. (21)], with β defined with the average OBS spacing along the array. When spacing variations are too large, thresholding of the singular value spectrum might be required to deduce a stable truncation.[17] Using the replica vectors $\boldsymbol{v}(\theta)$ defined in Eq. (15), the angular response $A(\theta)$ of a filter, $\boldsymbol{S}$, will be defined as

$$A(\theta) = ||\boldsymbol{S}\boldsymbol{v}(\theta)||_2 = \sqrt{\frac{1}{N}\sum_{i=1}^{N} |S_{ij}v_j(\theta)|^2}. \tag{32}$$

The response of the spatial filter, $\boldsymbol{S}^{1D}$, is shown in Fig. 4(d) for the band 10–40 Hz.

The value of β above which spatial aliasing appears depends on the grating lobe (Ref. 15, p. 54)

$$\beta = \frac{1}{1 + |\sin\theta|}, \tag{33}$$

where θ is the notch angle. For a notch filter with a null at $\theta = 90°$, aliasing starts at the design frequency ($\beta = 0.5$). Here the average spacing is ~26 m, therefore aliasing perturbs

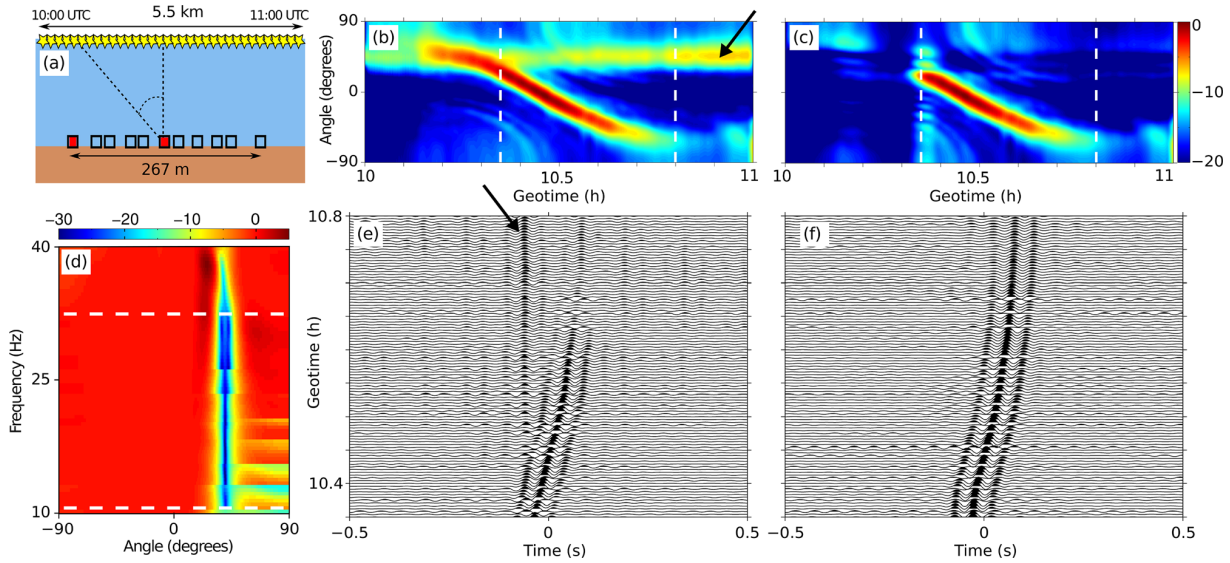

FIG. 4. (Color online) (a) Geometry of Gulf of Mexico active survey. The OBS 6 and 11 used in cross correlations are marked. (b) Broadband (11–33 Hz) plane-wave beamforming power output (dB) around the period of the active survey from 10:00 UTC. (c) Broadband (11–33 Hz) plane-wave beamforming power output (dB) when the STCM are spatially filtered [Eq. (6)] before beamforming. (d) Response (dB) of (truncated least-square) spatial filter with a stopband 10° wide centered on 40°. The frequency band 11–33 Hz considered in beamforming and crossc orrelations is within the dashed lines. (e) Time-domain cross correlations for OBS pair 6-11, zoomed in on the cross correlated direct arrivals from the active survey, between 10:21 and 10:48 UTC [dashed lines in (b) and (c)]. (f) Spatially filtered time-domain cross correlations for OBS pair 6-11, zoomed in on the cross correlated direct arrivals from the active survey, between 10:21 and 10:48 UTC [dashed lines in (b) and (c)]. The nearly constant power at about 40° [beamforming, (b)] and −0.06 s [cross correlations, (e)] is from the distant seismic survey that lasted the whole deployment (arrow).

significantly the filter response above $1514/(1+\sin 40^\circ)$ $26 \approx 35$ Hz [Eq. (33), with a sound speed of 1514 m/s, as measured *in situ*].

To obtain a notch deep enough (< -30 dB) to filter out the interferer, the filter was designed with the largest transition band possible that does not exceed the visible space boundary (90°). The discontinuity in the filter response is a side effect of the use of an integer index in the SVD truncation. Numerical tests show that choosing the integer above the rounded value leads to a smoother response without getting a positive gain (>0 dB) in the passband.

Above ~35 Hz, the stopband is aliased and the notch depth therefore is strongly reduced. Moreover, the use of the spatial filter in the aliasing regime is sensitive as it might attenuate preferred directions of arrival as well. At low frequencies (below 10 Hz), the array aperture in wavelengths is too small (less than 2) to provide good resolution. For these reasons, the processing here is restricted to the band 11–33 Hz.

Figure 4(c) illustrates broadband beamforming of the spatially filtered STCM averaged over this band. The interferer signal is completely nulled out. Although the active survey source and the interferer are not co-located, the spatial filter also attenuates the survey signal when the angle from the vertical is close to the rejection band, due to the cone ambiguity that is inherent with a 1D array.

The cross correlation processing was carried out as follows. The 1-h signals were segmented using a sliding time window of 15 s with 66% overlap. These short-term signals were Fourier transformed and multiplied in the spectral domain for all possible OBS pair combinations, leading to an ensemble of STCM. These STCM were spatially filtered [Eq. (7)] and then inverse Fourier transformed to go back to the time domain yielding the short-term cross correlations. Figures 4(e) and 4(f) illustrate the short-term cross correlations without and with spatial filtering, respectively, focusing on the direct arrival for OBS pair 6-11. This direct arrival goes from negative to positive times as the survey source progressively passes above the receiver pair. The peaks at ~0.06 s (arrow) are due to the distant seismic survey. These peaks are well attenuated by the spatial filter. Before 10.3 h, the interferer and active survey have comparable arrival angles and their associated peaks in the cross correlations are simultaneous. Therefore, the spatial filter also attenuates the direct arrivals from the active source of interest. A larger number of receivers and a more dense array would enable a narrower notch with similar depth, but would not avoid filtering out the survey source when vertical angle corresponds to interferer azimuth.

Similar to Eq. (1), an estimate of the EGF would be obtained by averaging the short-term cross correlations over the whole recording time.[37] The averaging process also can be made in the frequency domain [Eq. (4)] before inverse Fourier transform. Therefore, if no specific signal processing is carried out on the short-term cross correlations, the spatial filter can be applied to the ensemble averaged SCM [Eq. (7)].

2. Convex optimization based filter

The spatial filter can be obtained by solving a convex optimization problem; see Sec. III. Figure 5 shows the variation of the average notch depth over the notch interval ($40 \pm 5^\circ$) at 28 Hz as a function of the transition width and the passband fidelity constraint ϵ ($\beta \sim 0.5$ considering the average OBS spacing). The figure shows that a reduced transition width can be compensated by increasing ϵ.

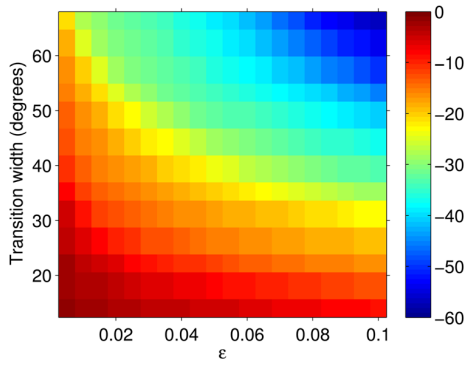

FIG. 5. (Color online) Average notch depth at 28 Hz obtained by convex optimization as a function of the transition width and the passband fidelity constraint ϵ, for the 11-element array in the Gulf of Mexico active survey. The constraint c_T is 1.1.

This feature is illustrated further by three different spatial filters with a similar notch design, but with different transition width and passband constraints. The transition width is defined relative to the half-power beamwidth (HPBW), where[15]

$$\text{HPBW} \approx 0.891 \frac{1}{\beta N}. \tag{34}$$

First, a wide transition width is allowed (1.85 × HPBW on each side of the rejection band) and a strong constraint on the passband fidelity is imposed ($\epsilon = 0.005$); see Fig. 6(a). Note that the transition width exceeds 90° below 28 Hz. Second, a narrower transition width is imposed (0.5 × HPBW on each side of the rejection band), but the constraint on passband fidelity is weaker ($\epsilon = 0.1$), so that the filter response still exhibits a deep notch; see Fig. 6(b). As a matter of comparison, the least-square solution for such reduced transition width has a maximum notch depth limited to −15 dB. The third case illustrates a frequency-independent transition band [1 × HPBW at $\beta = 0.5$ on each side of the rejection band, i.e., 10° (15°) on the left (right) side of the notch.]; see Fig. 6(c). To compensate for the progressive decrease of the transition width relative to the HPBW when decreasing the frequency, a frequency variable constraint is used in the convex optimization. The resulting spatial filter response exhibits a deep, well-focused notch over the rejection band across the whole frequency band, but with a reduced passband fidelity at low frequencies. In all cases, the constraint c_T was kept to 1.1. Varying this constraint has no significant effect on the solutions for these specific examples.

B. Upgoing/downgoing noise separation with a 2D array

The EGF between two receivers contains not only the direct path and water multiples, but also the reflections from

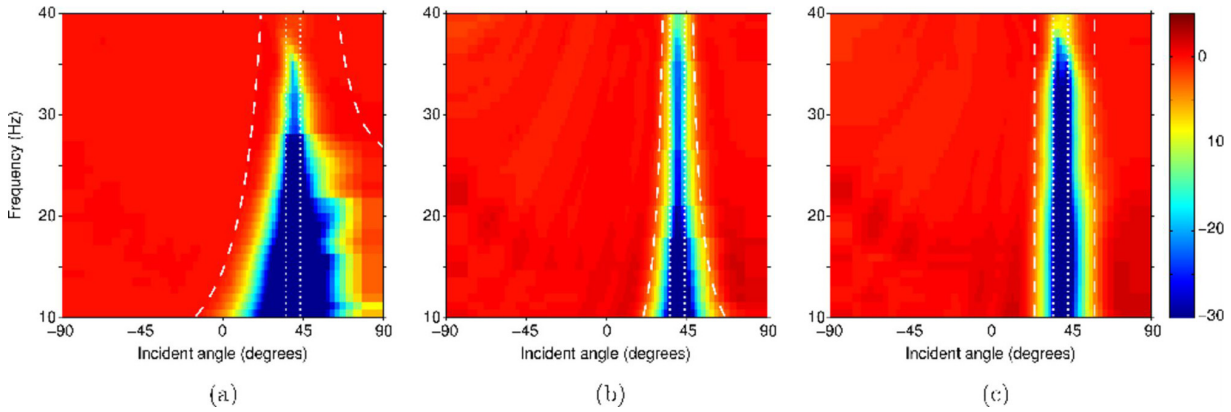

FIG. 6. (Color online) Response (dB) of the convex optimization designed spatial filters with a stopband 10° wide centered on 40° (dotted lines) and a total transition width (dashed lines) (a) equal to 3.7 × HPBW (frequency dependent), with the constraint $\epsilon = 0.005$; (b) equal to 1 × HPBW (frequency dependent), with the constraint $\epsilon = 0.1$; (c) equal to 25° (frequency-independent), with a frequency variable passband constraint (ϵ varies from 0.15 to 0.05). The constraint c_T is 1.1. The apparent asymmetry of the transition widths comes from their symmetric definition in $\sin(\theta)$ space.

bottom and subbottom layers. Spatial filters are here used to enhance reflected arrivals in the EGF in order to improve the estimates of the shallow subsurface reflectivity.

1. Simulation parameters

The use of a spatial filter with a 2D array is demonstrated here with simulated data. The environment is modeled as a water column of 200-m depth, with a constant sound speed of 1500 m/s, a first soft sediment layer of 50 m ($c = 1515$ m/s, $\rho = 1500$ kg/m^3, $\alpha = 0.2$ dB/λ), a second sediment layer of 75 m ($c = 1650$ m/s, $\rho = 1900$ kg/m^3, $\alpha = 0.8$ dB/λ) and a hard halfspace ($c = 2200$ m/s, $\rho = 2000$ kg/m^3, $\alpha = 0.1$ dB/λ). Shear waves are neglected. The frequency band is 50–250 Hz, the latter frequency is the design frequency of the array for 3-m spacing and a wave propagation speed of 1500 m/s. The receivers are on the bottom.

Acoustic propagation simulations are performed with the noise module of OASES.[38] The frequency domain CSDMs obtained from OASES are inverse Fourier transformed to estimate the EGF, according to Eqs. (1) and (2). The time series are gathered according to the distance between corresponding pair of receivers.

2. Upgoing/downgoing noise separation

When both pressure and vertical particle velocity measurements are available at the same location, e.g., as measured by OBS, the wavefield can be separated into upgoing (U) and downgoing (D) parts. Upgoing/downgoing (UD) separation is a standard seismic processing method used for removing the downgoing signals (typically the source signature) from the reflections (the upgoing signals).[22,23] UD separation applied to active cross correlation processing improves the quality of EGF estimates.[39]

The acoustic wavefield separation is obtained from the combination of the hydrophone and vertical particle velocity sensor in the frequency-wavenumber domain as[40]

$$p^{\mathrm{U}}(z;\,\omega,\,k_r) = \frac{1}{2}\left(p(z;\,\omega,\,k_r) - \frac{\rho\omega}{k_z} v_z(z;\,\omega,\,k_r)\right), \quad (35)$$

$$p^{\mathrm{D}}(z;\,\omega,\,k_r) = \frac{1}{2}\left(p(z;\,\omega,\,k_r) + \frac{\rho\omega}{k_z} v_z(z;\,\omega,\,k_r)\right), \quad (36)$$

where the vertical wavenumber is $k_z = \sqrt{(\omega^2/c^2) - k_r^2}$ and v_z is the vertical particle velocity. With active survey data, the UD separation is approximated by considering the incident angle, θ, for each shot, deduced from the source and receiver positions (e.g., Ref. 41)

$$k_z = \cos(\theta)\frac{\omega}{c}. \quad (37)$$

In a "passive" configuration, the source is diffuse. However, for noise from near vertical incidence ($\theta \sim 0$), $k_z \approx \omega/c$. Equations (35) are thus (omitting depth-dependence and frequency)

$$p^{\mathrm{U}} \approx \frac{1}{2}(p - \rho c v_z), \quad (38)$$

$$p^{\mathrm{D}} \approx \frac{1}{2}(p + \rho c v_z). \quad (39)$$

We consider an array of receivers capable of measuring the pressure and the vertical particle velocity. Assuming that arrivals far from near vertical incidence are reduced by a spatial bandpass filter, $\boldsymbol{S}_{2\mathrm{D}}$, using Eq. (5), we then can apply the approximate UD separation Eqs. (38) and (39) on each array receiver,

$$\tilde{\boldsymbol{p}}^{\mathrm{U}} \approx \frac{1}{2}(\tilde{\boldsymbol{p}} - \rho c\tilde{\boldsymbol{v}}_z) \;\; = \frac{1}{2}\boldsymbol{S}_{2\mathrm{D}}(\boldsymbol{p} - \rho c\boldsymbol{v}_z), \quad (40)$$

$$\tilde{\boldsymbol{p}}^{\mathrm{D}} \approx \frac{1}{2}(\tilde{\boldsymbol{p}} + \rho c\tilde{\boldsymbol{v}}_z) = \frac{1}{2}\boldsymbol{S}_{2\mathrm{D}}(\boldsymbol{p} + \rho c\boldsymbol{v}_z). \quad (41)$$

The approximated upgoing/downgoing CSDM is then

$$\begin{aligned}\tilde{\boldsymbol{R}}^{\mathrm{UD}} &= \mathbb{E}\left[\tilde{\boldsymbol{p}}^{\mathrm{U}}\tilde{\boldsymbol{p}}^{\mathrm{D}H}\right] \\ &= \frac{1}{4}\boldsymbol{S}_{2\mathrm{D}}\left[\boldsymbol{R}^{pp} - (\rho c)^2\boldsymbol{R}^{v_z v_z} + \rho c(\boldsymbol{R}^{pv_z} - \boldsymbol{R}^{v_z p})\right]\boldsymbol{S}_{2\mathrm{D}}^{H},\end{aligned} \quad (42)$$

where the superscript on each CSDM indicates the cross correlated components.

In the following example, a spatial filter, $\boldsymbol{S}_{2D}$, is designed for a square array of 10 by 10 elements. The element spacing is 3 m in both the x and y directions. The filter is designed to attenuate any contribution coming from an incident angle larger than $\theta = 25°$ [see Fig. 2(b)]. Since $\cos(25°) \approx 0.9$, the approximate UD separation Eqs. (38) and (39) is valid. The spatial filter is obtained using Eq. (12), where the pseudo-inverse uses the 2D truncation condition [Eq. (31)].

The angular response of $\boldsymbol{S}^{2D}$ is shown in Fig. 7. This filter is applied to the CSDMs to obtain the upgoing/downgoing CSDM [Eq. (42)].

On a single receiver, the arrivals are the direct arrival (no reflections in the source-receiver path), the primary reflected arrivals (each reflector), and the associated surface multiples. The cross correlation process between two receivers will give a peak for each combination of arrivals. Nevertheless, some of these peaks are not related to physical propagation of a wavefield through one receiver to the other, although a stationary-phase path exists. Compared to the actual Green's function between the two receivers, these *spurious* arrivals are artifacts coming from the cross correlation processing and are a characteristic of a surface noise sheet,[6,42] i.e., when noise sources do not completely surround the receivers. Such spurious arrivals should not be confused with peaks due to a discrete source, sometimes also referred to as spurious in the literature. Figure 8(a) illustrates the stationary-phase paths that lead to the EGF for two receivers on the seafloor with two subsurface reflectors. An example of a spurious stationary-phase path is shown in Fig. 8(b). Other types of spurious combinations exist, in particular, the *spurious multiples*,[42] arising from the cross correlation of the reflected wavefield from different interfaces on each receiver.

The noise cross correlations for pressure and vertical particle velocity (not filtered) are gathered in Figs. 9(a) and 9(b). The pressure cross correlations show weak reflection peaks, especially for the second reflector. On the other hand, particle velocity cross correlations exhibit higher amplitudes

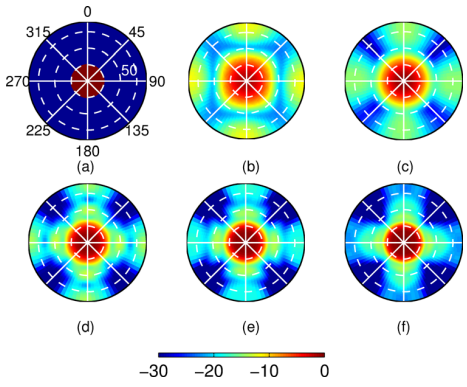

FIG. 7. (Color online) (a) Ideal spatial filter. Angular response (dB) of truncated least-square spatial filters at (b) 50, (c) 100, (d) 150, (e) 200, and (f) 250 Hz [Eq. (32), with N being equal to the total number of sensors]. The polar angle corresponds to the azimuth ϕ, from 0–360°. The radial axis corresponds to elevation θ [see Fig. 2(b)], from 0–90° (dashed circles).

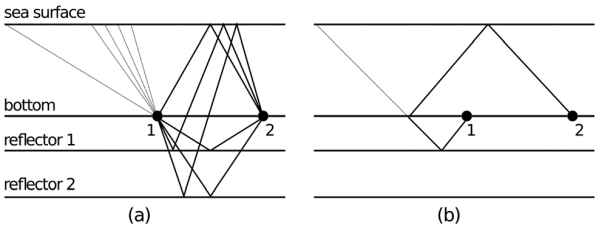

FIG. 8. Schematic representation of stationary-phase paths for two receivers on the seafloor and source at the sea surface, neglecting refraction. (a) Stationary-phase paths given by the cross correlation of direct arrivals on receiver 1 and all other types of arrivals on receiver 2 (reflected or multiples). (b) Example of a spurious arrival, here corresponding to the cross correlation of a reflected arrival on receiver 1 and a surface multiple on receiver 2.

for reflection-related peaks, but are accompanied by higher amplitudes for the spurious arrivals, resulting in traces that are difficult to interpret as many arrival times cannot be directly associated with a reflector. Note also the decreasing amplitude of direct arrivals [forming the "V" in Figs. 9(a) and 9(b)] with the receiver separation which is related to the vertical sensitivity of vertical particle velocity sensors. The filtered upgoing/downgoing cross correlations obtained from the inverse Fourier transform of Eq. (42) are shown in Fig. 9(c). The direct arrivals (close to horizontal) are removed by the filtering process. The spurious arrivals are eliminated from one side of the cross correlations so that only the "real" arrivals that can be associated with reflectors remain, here on the positive time side [shaded area in Fig. 9(c)]. Surface multiples are attenuated but not removed as part of the downgoing energy reaching the second receiver of the cross correlated pair is reflected by the seafloor. Even in the case of a uniform noise source distribution, the EGF extracted from the upgoing/downgoing CSDM is not an antisymmetric function with respect to time.

VI. DISCUSSION

The feasibility of spatial filtering depends strongly on the array aperture and the number of receivers (or, equivalently, the receiver spacing). These parameters limit the frequency band that can be filtered effectively. The response at lower frequencies is poor due to the limited aperture in wavelengths. Increasing the array aperture improves the angular resolution. Above the design frequency, spatial aliasing is introduced, so that arrivals expected to pass might be filtered out due to grating lobes.

The formulation of matrix spatial filters for 2D arrays is similar to the 1D case[16–18] and only differs in the steering matrix definition and its associated SVD. However, 1D beamforming suffers from azimuthal ambiguity around the array axis; therefore, a horizontal array steered vertically still will receive horizontally propagating noise. Thus, the UD separation process Eqs. (38) and (39) cannot be applied to a 1D array.

The truncation of the singular values in the pseudo-inverse [Eq. (13)] is critical for obtaining a useful filter response. If singular values that are too small are kept, the filter is unstable and can result in a gain that is too large in the passband. However, the truncation index is less critical for 2D arrays as the spectrum exhibits slower decay

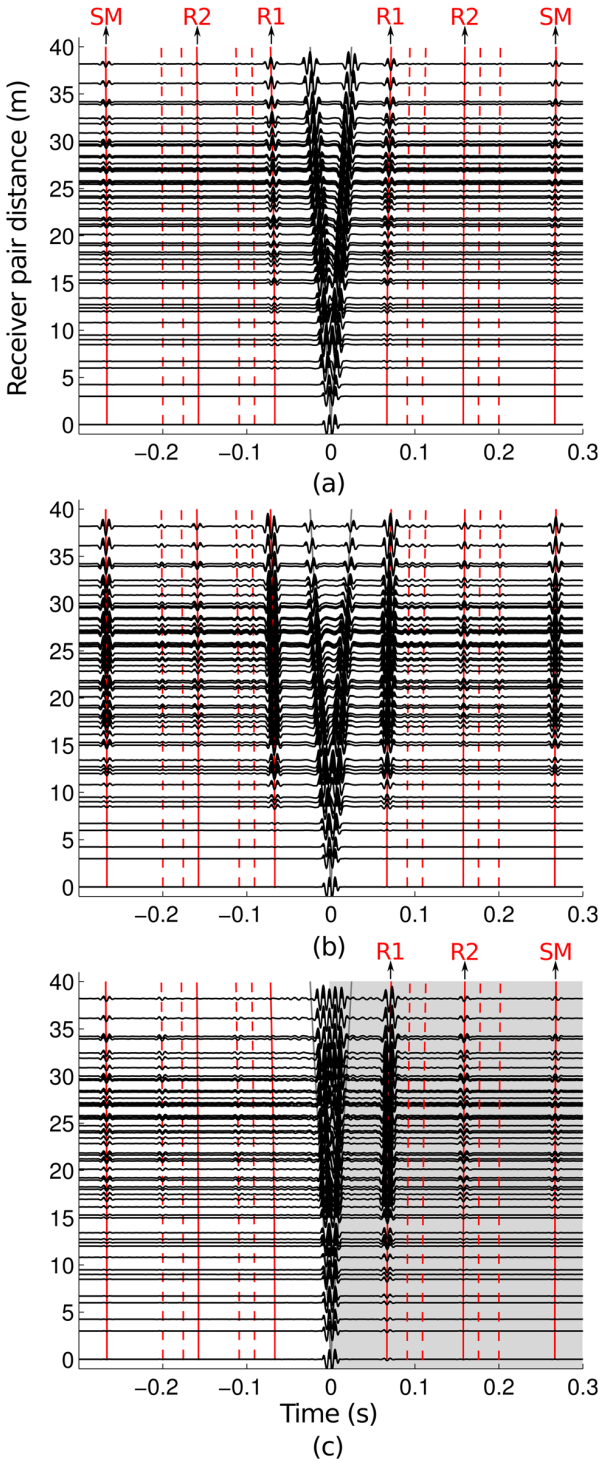

FIG. 9. (Color online) Pressure (a) and vertical particle velocity (b) EGF extracted from surface noise on a 2D array of 10 by 10 elements on the seafloor. (c) Upgoing/Downgoing EGF after truncated least-square spatial filtering [Eq. (42)]. The theoretical arrival times (overlaid vertical lines) are from a ray-tracing code: "Real" arrivals are in solid lines [reflector 1 (R1), reflector 2 (R2), and surface multiple (SM)], spurious arrivals are in dashed lines.

compared to 1D arrays. On the other hand, if the singular value spectrum is truncated too much, the filter response typically shows unwanted notches because some of the singular vectors corresponding to the visible space are missing.

The flexibility of the convex optimization approach is attractive, especially because it might lead to deeper notch depths and smoother dependence on frequency than in the least-square solution. Given the availability of efficient solvers that readily can be used, the simplicity of its implementation clearly is an advantage. However, the computational burden is significantly larger which makes the use of a convex optimization approach for larger arrays and a wide band difficult to implement (e.g., arrays with hundreds of sensors such as the USArray). For instance, the central processing unit time required to obtain the spatial filters illustrated in Fig. 6 by convex optimization (30 min on a dual-core 2.4 GHz computer) is 3 orders of magnitude longer than for an equivalent least-square design.

Finding good values for the constraints and the transition width is based on a trial-and-error approach. Passband constraint values that are too small or a transition width that is too narrow might inhibit the solver finding an optimal solution.

When stable truncation indices are used for the least-square inversion, the filter response does not exhibit positive gain. This is not the case with the convex optimization result because the passband constraint formulation only restricts the amplitude of the oscillations *around* 0 dB. Thus, it is important to maintain good fidelity in the passband ($\epsilon \approx 0$) to prevent artificial amplification of some directions of arrival.

VII. CONCLUSION

The extraction of Green's functions from noise cross correlations is often biased by interferers from arbitrary directions. Matrix-based spatial filters are used here for filtering the cross correlations between receivers using a data and model independent approach. Stable broadband filters are obtained by analytically deriving the frequency-dependent low-rank approximation of the pseudo-inverse involved in the filter design procedure for linear (1D) and planar (2D) regularly spaced arrays.

Matrix filters can be designed with flexibility in the selection of the performance criteria in the rejection band, transition band, and passband. Using this approach the filter easily can be found using convex optimization.

A spatial filter was shown to attenuate effectively interference from a discrete source in a linear array case. With planar arrays, spatial filters enable focusing the array vertically. When pressure and vertical particle velocity signals are both measured at each receiver, an approximate upgoing/downgoing wavefield separation procedure separates efficiently real and spurious arrivals.

Although the results presented here are in the context of underwater acoustics, similar spatial filters might be used for seismic arrays for focusing on specific directions of arrival.

ACKNOWLEDGMENTS

The Office of Naval Research (Grant No. N00014-11-0320) supported this work. The authors thank R. Menon for helpful discussions.

[1]M. J. Buckingham, B. V. Berknout, and S. A. L. Glegg, "Imaging the ocean with ambient noise," Nature **356**, 327–329 (1992).

[2]O. I. Lobkis and R. L. Weaver, "On the emergence of the Green's function in the correlations of a diffuse field," J. Acoust. Soc. Am. **110**, 3011–3017 (2001).
[3]R. Snieder, "Extracting the Green's function from the correlation of coda waves: A derivation based on stationary phase," Phys. Rev. E **69**, 046610 (2004).
[4]P. Roux, K. G. Sabra, W. A. Kuperman, and A. Roux, "Ambient noise cross correlation in free space: Theoretical approach," J. Acoust. Soc. Am. **117**, 79–84 (2005).
[5]L. A. Brooks and P. Gerstoft, "Ocean acoustic interferometry," J. Acoust. Soc. Am. **121**, 3377–3385 (2007).
[6]L. A. Brooks and P. Gerstoft, "Green's function approximation from cross-correlation of active sources in the ocean," J. Acoust. Soc. Am. **126**, 46–55 (2009).
[7]M. J. Buckingham, "On the two-point cross-correlation function of anisotropic, spatially homogeneous ambient noise in the ocean and its relationship to the Green's function," J. Acoust. Soc. Am. **129**, 3562–3576 (2011).
[8]S. C. Walker, "A model for spatial coherence from directive ambient noise in attenuating, dispersive media," J. Acoust. Soc. Am. **132**, EL15–EL21 (2012).
[9]M. J. Buckingham, "Cross-correlation in band-limited ocean ambient noise fields," J. Acoust. Soc. Am. **131**, 2643–2657 (2012).
[10]V. C. Tsai, "On establishing the accuracy of noise tomography travel-time measurements in a realistic medium," Geophys. J. Int. **178**, 1555–1564 (2009).
[11]R. Menon, P. Gerstoft, and W. S. Hodgkiss, "Cross-correlations of diffuse noise in an ocean environment using eigenvalue based statistical inference," J. Acoust. Soc. Am. **132**, 3213–3224 (2012).
[12]O. Carrière and P. Gerstoft, "Deep-water subsurface imaging using OBS interferometry," Geophysics **78**, Q15–Q24 (2013).
[13]T. Gallot, S. Catheline, P. Roux, and M. Campillo, "A passive inverse filter for Green's function retrieval," J. Acoust. Soc. Am. **131**, EL21–EL27 (2012).
[14]C. Leroy, S. Lani, K. G. Sabra, W. S. Hodgkiss, W. A. Kuperman, and P. Roux, "Enhancing the emergence rate of coherent wavefronts from ocean ambient noise correlations using spatio-temporal filters," J. Acoust. Soc. Am. **132**, 883–893 (2012).
[15]H. L. Van Trees, *Optimum Array Processing (Detection, Estimation, and Modulation Theory, Part IV)* (Wiley-Interscience, New York, 2002), Chaps. 2–4.
[16]C. MacInnes, "Source localization using subspace estimation and spatial filtering," IEEE J. Ocean. Eng. **29**, 488–497 (2004).
[17]S. A. Stotts, "A robust spatial filtering technique for multisource localization and geoacoustic inversion," J. Acoust. Soc. Am. **118**, 139–162 (2005).
[18]T. B. Neilsen, "Localization of multiple acoustic sources in the shallow ocean," J. Acoust. Soc. Am. **118**, 2944–2953 (2005).
[19]R. Vaccaro and B. Harrison, "Optimal matrix-filter design," IEEE Trans. Signal Process. **44**, 705–709 (1996).
[20]P. Gerstoft and W. S. Hodgkiss, "Improving beampatterns of two-dimensional random arrays using convex optimization," J. Acoust. Soc. Am. **129**, EL135–EL140 (2011).
[21]S.-P. Wu, S. Boyd, and L. Vandenberghe, "FIR filter design via spectral factorization and convex optimization," in *Applied and Computational Control, Signals, and Circuits*, edited by B. N. Datta (Birkhäuser, Boston, MA, 1999), pp. 215–245.
[22]D. Loewenthal, S. S. Lee, and G. H. F. Gardner, "Deterministic estimation of a wavelet using impedance type technique," Geophys. Prospect. **33**, 956–969 (1985).
[23]L. Amundsen and A. Reitan, "Decomposition of multicomponent sea-floor data into upgoing and downgoing P- and S-waves," Geophysics **60**, 563–572 (1995).
[24]M. Siderius, C. H. Harrison, and M. B. Porter, "A passive fathometer technique for imaging seabed layering using ambient noise," J. Acoust. Soc. Am. **120**, 1315–1323 (2006).
[25]J. Traer, P. Gerstoft, and W. S. Hodgkiss, "Ocean bottom profiling with ambient noise: A model for the passive fathometer," J. Acoust. Soc. Am. **129**, 1825–1836 (2011).
[26]H. Yao, P. Gerstoft, P. M. Shearer, and C. Mecklenbräuker, "Compressive sensing of the Tohoku-Oki Mw 9.0 earthquake: Frequency-dependent rupture modes," Geophys. Res. Lett. **38**, L20310 (2011).
[27]S. de Ridder and J. Dellinger, "Ambient seismic noise eikonal tomography for near-surface imaging at Valhall," The Leading Edge **30**, 506–512 (2011).
[28]S. Boyd and L. Vandenberghe, *Convex Optimization* (Cambridge University Press, New York, 2004), Chaps. 1–7.
[29]B. D. Van Veen and K. M. Buckley, "Beamforming: A versatile approach to spatial filtering," IEEE ASSP Magazine **5**, 4–24 (1988).
[30]B. F. Cron and C. H. Sherman, "Spatial-correlation functions for various noise models," J. Acoust. Soc. Am. **34**, 1732–1736 (1962).
[31]P. Gerstoft, R. Menon, W. S. Hodgkiss, and C. F. Mecklenbräuker, "Eigenvalues of the sample covariance matrix for a towed array," J. Acoust. Soc. Am. **132**, 2388–2396 (2012).
[32]R. M. Gray, "Toeplitz And circulant matrices: A review," Found. Trends. Commun. Inf. Theory **2**, 155–239 (2005).
[33]G. N. Watson, *A Treatise on the Theory of Bessel Functions* (Cambridge University Press, New York, 1944), Chap. 2.
[34]P. Voois, "A theorem on the asymptotic eigenvalue distribution of Toeplitz-block-Toeplitz matrices," IEEE Trans. Signal Process. **44**, 1837–1841 (1996).
[35]N. Baddour, "Operational and convolution properties of two-dimensional Fourier transforms in polar coordinates," J. Opt. Soc. Am. A **26**, 1767–1777 (2009).
[36]A. D. Poularikas, *Transforms and Applications Handbook* (CRC Press, New York, 2010), Chap. 9.
[37]L. A. Brooks and P. Gerstoft, "Green's function approximation from cross-correlations of 20–100 Hz noise during a tropical storm," J. Acoust. Soc. Am. **125**, 723–734 (2009).
[38]H. Schmidt, "OASES version 3.1 user guide and reference manual," Department of Ocean Engineering Massachusetts Institute of Technology, Cambridge, MA (2011), available at http://oceanai.mit.edu/lamss/docs/oases_manual.pdf (Last viewed 06/21/2013).
[39]K. Mehta, A. Bakulin, J. Sheiman, R. Calvert, and R. Snieder, "Improving the virtual source method by wavefield separation," Geophysics **72**, V79–V86 (2007).
[40]L. Amundsen, "Wavenumber-based filtering of marine point-source data," Geophysics **58**, 1335–1348 (1993).
[41]M. M. Backus, P. E. Murray, B. A. Hardage, and R. J. Graebner, "High-resolution multicomponent seismic imaging of deepwater gas-hydrate systems," The Leading Edge **25**, 578–596 (2006).
[42]R. Snieder, K. Wapenaar, and K. Larner, "Spurious multiples in seismic interferometry of primaries," Geophysics **71**, SI111–SI124 (2006).